An Adaptive Wavelet–Vaguelette Algorithm for the Solution of PDEs

Jochen Fröhlich*,1 and Kai Schneider†,2

*Konrad–Zuse–Zentrum Berlin, Heilbronner Str. 10, 10711 Berlin, Germany; †Fachbereich Chemie, Technische Chemie, Universität
Kaiserslautern, Erwin–Schrödinger Straße, 67663 Kaiserslautern, Germany

The paper first describes a fast algorithm for the discrete orthonormal wavelet transform and its inverse without using the scaling function. This approach permits to compute the decomposition of a function into a lacunary wavelet basis, i.e., a basis constituted of a subset of all basis functions up to a certain scale, without modification. The construction is then extended to operator-adapted biorthogonal wavelets. This is relevant for the solution of certain nonlinear evolutionary PDEs where a priori information about the significant coefficients is available. We pursue the approach described in (J. Fröhlich and K. Schneider, *Europ. J. Mech. B/Fluids* 13, 439, 1994) which is based on the explicit computation of the scalewise contributions of the approximated function to the values at points of hierarchical grids. Here, we present an improved construction employing the cardinal function of the multiresolution. The new method is applied to the Helmholtz equation and illustrated by comparative numerical results. It is then extended for the solution of a nonlinear parabolic PDE with semi-implicit discretization in time and self-adaptive wavelet discretization in space. Results with full adaptivity of the spatial wavelet discretization are presented for a one-dimensional flame front as well as for a two-dimensional problem.   © 1997 Academic Press

1. INTRODUCTION

In recent years the development of multiresolution techniques and wavelets has had a tremendous impact on signal and image processing and many other fields. One of them is the numerical solution of partial differential equations where related ideas have been popular for a long time. Speaking of a PDE we have in mind a partial differential equation with one or more dimensions in space and a time derivative such as typical for conservation laws. Below, the derivative in time is generally discretized by a finite difference scheme while a wavelet discretization is used in space.

It is beyond the scope of this introduction to survey all the relevant literature on the application of wavelets to PDEs. A recent attempt has been made by Jawerth and Sweldens [29] to which the reader is referred for more comparative information. The currently existing algorithms can be classified in different ways. First of all, we can distinguish between Galerkin or Petrov–Galerkin schemes, collocation schemes, and algebraic methods. By the latter we mean algorithms which start from a classical discretization, e.g., by finite differences in space. Wavelets are then used in the following stages to speed up the linear algebra. On the other hand, the former two schemes employ wavelets or wavelet-like functions directly for the discretization of the solution and the operators which then induces the subsequent linear algebra.

Another classification can be made according to whether a wavelet representation is used for the efficient representation of an operator, the compressed representation of the solution or for both. The first family comprises the "decomposition schemes." They are based on the fact that wavelets are well localized in physical space and in Fourier space. Hence, an operator which does not too much perturb this localization has, for a given precision, a sparse representation in this basis. It also allows efficient diagonal preconditioning as first observed by Jaffard [28]. Several papers such as [16] have exploited this property of a wavelet basis which can be viewed as a particular multilevel scheme. In [15] a further step has been made incorporating a homogeneous elliptic differential operator into the construction of a biorthogonal basis. Used in a Petrov–Galerkin method it generates a block-diagonal matrix. A remarkable fact when employing wavelets for the discretization of Calderon–Zygmund operators is that both, the operator and its inverse have a sparse representation [37]. The BCR algorithm [6] is an algorithm which can be used to benefit from this fact. Starting from a given matrix it generates a sparse, compressed representation of this matrix which then speeds up linear algebra. When, e.g., resulting from the discretization of a usual difference operator powers of the compressed matrix are even more sparse. This has been used in [21, 1] for linear evolution equations. We subsume the cited methods (and others not mentioned

---

[1] Present address: Institut für Hydromechanik, Universität Karlsruhe, Kaiserstraße 12, 76128 Karlsruhe, Germany.

[2] Present address: Institut für Chemische Technik, Universität Karlsruhe, Kaiserstraße 12, 76128 Karlsruhe, Germany.

here for lack of space) as "decomposition schemes" since they start from a regular structure, a uniform discretization or a given matrix, and employ a certain multilevel decomposition which then allows preconditioning or fast algebra. The underlying regular discretization, however, is still present.

Although in principle the wavelet multilevel decomposition of the operator could be used in connection with an adaptive decomposition of the solution this is straightforward only for relatively few wavelet methods. Some of these are the "adaptive evaluation schemes." They are characterized by the fact that the solution is discretized in an adaptive wavelet basis and that a discretized differential operator is applied to the nonuniform unknowns. This typically occurs with explicit time discretization. Examples are [2], the collocation method of [11] based on a particular Sobolev inner product, and the seminal work of Harten [25]. In [26] a broad multiresolution framework is developed which allows to incorporate existing algorithms for hyperbolic conservation laws.

The third class of methods are the "adaptive inversion schemes" using simultaneously an adaptive discretization of the unknown and a sparse representation of the operator. Elementary ones such as [34] set up a Galerkin matrix for an adaptive wavelet representation of the solution with the system then to be solved by a standard method. A similar approach is made by [4] using the interpolatory multiresolution of [20] to define an adaptive collocation scheme and to incorporate boundary conditions. The price for the interpolatory basis, however, is that diagonal preconditioning in this basis does not yield bounded condition number [5]. In [49] the authors have developed a similar multilevel collocation method with a linear system to be solved on each level. An early attempt to exploit the compression of the operator and its inverse in a wavelet basis as well as adaptive wavelet representation of the solution has been made in [33] using the theoretical results of [48]. The present work is to be viewed in this line. A different approach has been taken by Perrier and Charton [12] which use an algebraic wavelet method, based on a finite difference scheme, to compress the discrete inverse operator and the actual solution during the time advancement.

In all of the three families we find Galerkin, collocation, and algebraic methods or some sort of hybrid approaches. Galerkin schemes potentially allow easier incorporation of the operator into the basis construction, better preconditioning, and are more accessible to theoretical analysis. On the other hand, adaptive transforms and boundary conditions can easier be realized with collocation. The cited collocation schemes, however, generally give up the condition of vanishing moments which may have undesirable consequences. Although starting from different discretization many of the resulting algorithms exhibit similar features. Under certain uniformity conditions Gomes [24]

showed that some Galerkin and collocation schemes are equivalent and gives their relation to the method of Harten. When dealing with adaptive discretizations, or boundary conditions, one or the other kind of approach may, however, have conceptual and practical advantages.

The present algorithm is an "adaptive inversion scheme." It employs semi-implicit time discretization for a parabolic PDE and is direct. No linear system needs to be solved due to diagonalizing the stiffness matrix through an appropriate choice of test and trial functions in a Petrov–Galerkin method. The adaptive discretization exploits the compression property of wavelets. In contrast to most signal processing tasks, however, avoiding a costly regular fine grid for the solution of a PDE requires a bottom–up strategy of successive local refinements. Only the subset of the relevant amplitudes is to be computed. This loss of regularity in the index set is an essential difficulty of the approach which we overcome in a particular way in the present paper. Recall that the classical Mallat algorithm can no longer be employed in the lacunary case as it is based on the use of the scaling functions' coefficients on each scale which do not exhibit the same lacunarity as the wavelet coefficients. In that case it is not clear how to define a suitable projection on the lacunary basis.

Let us note that the need of repeated transforms between physical space, i.e., the values at certain grid points and coefficient space, originates in the nonlinearity of the PDE to be solved. For linear operations such as derivation, multiplication by powers of the independent variable etc. the conversion to operations on the wavelet coefficients is possible [31, 21]. For simple nonlinearities the approximate evalution in coefficient space has been studied by Beylkin [7] and others. But for general nonlinear terms such as encountered in combustion modeling the evaluation in physical space seems to be unavoidable.

Different strategies to cope with locally refined wavelet basis have been developed. Plantevin [39] constructs an orthonormal basis for a given locally refined dyadic grid. As each modification of the grid requires a new basis construction this can become very costly and seems not to be appropriate for the use in the adaptive discretization of unsteady solutions of PDEs. Ponenti [40] aims at retaining as much of the unmodified compactly supported wavelet basis as possible and succeeds in modifying only those functions that live near the border of the index set of retained wavelets. However, the projection step onto the space spanned by these functions is left unconsidered. Sweldens [46] has developed a strategy which allows almost arbitrary spacing of grid points. A completely irregular discretization, however, makes it difficult to take into account differential operators and to consider smooth bases.

The present construction retains the wavelet basis as it is. A lacunary subset is accessed through a simple hierarchical subtraction strategy which permits us to compute individ-

ual coefficients of the wavelet series with linear operation count [22]. We give a detailed description of the algorithm for a pure wavelet decomposition and improve the former algorithm by employing the cardinal Lagrange function. This is important as it results in speedup, facilitates the implementation, and allows a clearer analysis of the procedure. Up to here, the approach is similar to the partial collocation method briefly sketched in [35] and the multi-level collocation for frames of [49]. The next important step is to incorporate the differential operator into the basis. Thereby, the related stiffness matrix is diagonalized, avoiding its assembly and inversion. This is particularly favorable when frequently changing the set of active basis functions. We show how the hierarchical decomposition into a lacunary basis of the first part can be adapted to this situation. Thereby, we arrive at an interpolatory transform for a fully adaptive operator–orthogonal wavelet–vaguelette decomposition. It is implemented to solve elliptic problems in one and two space dimensions with periodic boundary conditions. In a final step the algorithm is applied to unsteady reaction–diffusion problems, where the semi-implicit time discretization requires the solution of an elliptic problem in each time step. The set of relevant coefficients to be computed is furnished by a dynamic adaption strategy in coefficient space.

The paper is organized as follows. We start in Section 2 with the case of a pure wavelet decomposition and introduce the relevant notation and properties. Furthermore, the inverse transform described here will be retained later on in the complete algorithm. In Section 3 we develop the wavelet–vaguelette decomposition and demonstrate its relation to PDEs. For clearness and ease of notation the method is outlined in these first sections considering the real line. The practical implementation, however, makes use of periodicity. Hence assembling some remarks related to this topic in a separate section seems to be appropriate (Section 4). With the ground prepared in such a way the description of the two-dimensional algorithm in Section 5 can be rather brief. In Section 6 we investigate the essential decay properties of the employed basis function by means of numerical experiments. We finally report sample computations for one- and two-dimensional flames which illustrate the properties of the presented method.

2. RECURSIVE INTERPOLATORY TRANSFORM FOR ORTHOGONAL WAVELETS

The following approach is by no means restricted to orthonormal wavelets but can rather be applied to any basis exhibiting scale separation (even when this only holds in a qualitative way as in [9]). Since orthogonality of the employed basic wavelets is crucial for the later discretization of a PDE we formulate it in these terms right from the beginning.

Assume the set of closed subspaces $\{V_j\}_{j \in \mathbb{Z}}$ with $V_j \subset V_{j+1}$ being a multiresolution analysis (MRA) of $L^2(\mathbb{R})$ with scalar product $\langle ., . \rangle$ and norm $\|.\|_2$. Let this MRA be generated by some function $b(x)$ through dyadic dilation and translation, i.e.,

$$b_{j,k}(x) = 2^{j/2} b(2^j x - k) \tag{2.1}$$

with $\{b_{j,i}\}_i$ constituting a Riesz basis of V_j, not necessarily being orthogonal. The index convention for other functions below will often be slightly different from (2.1) but made precise each time. Dropping an index means setting it to zero, such as $b_j = b_{j,0}$, $b = b_0$. The orthonormal scaling function and wavelet function for this MRA are denoted ϕ and ψ, respectively. The function ϕ can be obtained from b through orthonormalization, but occasionally we also set $b = \phi$ right from the start. Furthermore, we suppose that ψ has $M + 1$ vanishing moments. Due to the MRA structure any function $f_J \in V_J$ can be written as

$$f_J(x) = \sum_k c_{J,k} \phi_{J,k}(x) = \sum_k c_{0,k}(x) + \sum_{j=0}^{J-1} \sum_k d_{j,k} \psi_{j,k}(x), \tag{2.2}$$

employing (2.1) for the definition of shift and scale index. Bounds for the translation indices are left unspecified throughout, as these will later be governed by the periodization. The index $j = 0$ for the coarsest scale in (2.2) is arbitrary and chosen for later convenience. The filters

$$G_n^j = \langle \phi_{j,n}, \psi_{j-1,0} \rangle, \quad H_n^j = \langle \phi_{j,n}, \phi_{j-1,0} \rangle \tag{2.3}$$

are classically used for the transition between both representations in (2.2). They can be obtained in physical space for compactly supported bases and in Fourier space through

$$\hat{H}^*(\omega) = \hat{\phi}(2\omega)/\hat{\phi}(\omega), \quad \hat{G}^*(\omega) = \hat{\psi}(2\omega)/\hat{\phi}(\omega), \tag{2.4}$$

where the notation of the Appendix, Eq. (A.5), is employed to emphasize the periodicity of these expressions with respect to ω. Given a function $f \in L^2(\mathbb{R})$, a projection P_J has to be applied to obtain $f_J = P_J f$. At this point there exists a certain liberty. In [47] different quadrature formulas are developed for this task. The algorithms below rely on the collocation projection as it allows easy connection to values in physical space and successive coarsening of the employed grids. It is defined by

$$f_J\left(\frac{k}{2^J}\right) = f\left(\frac{k}{2^J}\right). \tag{2.5}$$

Hence, f_J in (2.2) is determined through

$$f_J(x) = \sum_k f\left(\frac{k}{2^J}\right) S_J\left(x - \frac{k}{2^J}\right) \qquad (2.6)$$

with the cardinal Lagrange function S_J of V_J defined by

$$S_J\left(\frac{i}{2^J}\right) = \delta_{i,0}, \quad V_J = \overline{\mathrm{span}}\left\{S_{J,k} = S_J\left(x - \frac{k}{2^J}\right)\right\}_k. \quad (2.7)$$

(The scale index for this function is defined without the factor $2^{j/2}$ for ease of notation.) Combining (2.2) and (2.6), the coefficients $c_{J,k}$ in (2.2) are computed by application of the interpolation filter

$$I_n^J = \langle S_{J,n}, \phi_{J,0}\rangle, \ \ \widehat{I^J*}(\omega) = 2^{-J/2}\,\hat{I}*\left(\frac{\omega}{2^J}\right), \ \ \hat{I}*(\omega) = \hat{S}(\omega)/\hat{\phi}(\omega) \quad (2.8)$$

to the sampled values $\{f(k/2^J)\}_k$.

Note that when using wavelets for the discretization of a PDE one would like to exploit the regularity of these functions to obtain efficient approximation of smooth solutions. If, however, the projection step has a truncation error of order much lower than this regularity, it is useless to employ regular wavelets. The classical projection $c_{J,i} = f(x_{J,i})$ to determine f_J in (2.2), for example, converges only like $O(h)$ with $h = 2^{-J}$. Let us remark that in the L^2 setting considered so far interpolation has no meaning. However, as soon as the basis functions have sufficient regularity the same multiresolution can be viewed as a multiresolution in the L^2-Sobolev space H^r of order $r \geq 1$ without any further change [3].

The existence of a cardinal Lagrange function S_J of V_J is guaranteed by

PROPOSITION 1. [50]. *For a reproducing kernel Hilbert space V spanned by a Riesz basis $\{b(x - k)\}_{k\in\mathbb{Z}}$ such that $\hat{b}*(\omega) \neq 0$, a cardinal Lagrange function exists and is given by*

$$\hat{S}(\omega) = \frac{\hat{b}(\omega)}{\hat{b}*(\omega)}, \quad \omega \in \mathbb{R}. \qquad (2.9)$$

Remark. In [50] the assertion is first proved for $b = \phi$ constituting the kernel of the reproducing kernel Hilbert space V. Equation (2.9) then is deduced as Riesz bases can be converted from one into the other and since S is unique modulo discrete shifts. For spline spaces this equation has already been used by Schoenberg [43].

Consider the points of nested dyadic grids in $\mathbb{R}$

$$x_{j,i} = \frac{i}{2^j}, \quad i, j \in \mathbb{Z} \qquad (2.10)$$

verifying the trivial recursion

$$x_{j+1,2i} = x_{j,i}, \quad x_{j+1,2i+1} = \tfrac{1}{2}x_{j,i} + \tfrac{1}{2}x_{j,i+1}. \qquad (2.11)$$

In the following the cardinal interpolation function will play the role of the scaling function employed in the classical algorithm. We therefore define the filters

$$D_m^j = \langle S_{j,m}, \psi_{j-1,0}\rangle \qquad (2.12)$$

representing collocation projection onto V_j and subsequent projection onto W_{j-1} when applied to the values $\{f(x_{j,i})\}_i$. Similar to recursions in j for $\widehat{H^j}$, $\widehat{G^j}$ one can show

PROPOSITION 2. *The filters D^j in (2.12) verify the recurrence relation*

$$(\widehat{D^{j-1}})*(\omega) = 2^{3/2}(\widehat{D^j})*(2\omega), \quad \omega \in \mathbb{T}. \qquad (2.13)$$

Proof. Equations (2.3), (2.8), (2.12) yield

$$D_m^j = \sum_l G_l^j I_{l-m}^j. \qquad (2.14)$$

Transfer to Fourier space and application of (2.4) and (2.8) back and forth for $j - 1$ and j, respectively, gives the assertion. ∎

The following theorem describes the biorthogonality of the filter D^J with respect to sampled wavelets and scaling functions.

PROPOSITION 3. *Given ψ_{ji}, S_{ji}, and D_n^J defined by (2.12). Then*

$$\text{(i)} \quad \sum_n D_{n-2k}^J \psi_{j,l}(x_{J,n}) = \delta_{j,J-1}\delta_{l,k}, \quad j < J, \quad (2.15)$$

$$\text{(ii)} \quad \sum_n D_{n-2k}^J S_{j,l}(x_{J,n}) = 0, \qquad j < J, \quad (2.16)$$

where $\delta_{i,k}$ is the Kronecker symbol.

Proof. (i) The sampling theorem in V_J yields

$$\psi_{j,l}(x) = \sum_n \psi_{j,l}\left(\frac{n}{2^J}\right) S_{J,n}(x), \quad j < J. \qquad (2.17)$$

Applying scalar products with $\psi_{J-1,\mathrm{k}}$ on both sides and using (2.12), together with the orthogonality of the wavelets proves (2.15).

(ii) Analogously, starting from

$$S_{j-1,k}(x) = \sum_i S_{j-1,k}\left(\frac{i}{2^J}\right) S_{J,i}(x) \qquad (2.18)$$

with $j < J$ and using the orthogonality of $\psi_{J-1,i}$ with respect to functions in V_j with $j < J$, Eq. (2.16) is proved. ∎

COROLLARY 1.

$$\sum_n n^k D_n^j = 0, \quad k = 0, ..., M; \quad j \in \mathbb{Z} \qquad (2.19)$$

Proof. Equation (2.19) follows from (2.17) with $\psi(x)$ replaced by x^k. Scalar products with $\psi_{J-1,k}$ on both sides allow us to use the moment conditions for ψ. ∎

The above shows that, in fact, the filters D^j correspond to finite difference formulas of order $M + 1$. With the present construction these filters generally do not have compact support which results in most cases from the appearance of the cardinal function. In particular, their decay is algebraic for the multiresolutions of Meyer wavelets employed below and exponential for spline wavelets. The latter also holds for Daubechies wavelets since their cardinal function has noncompact support and decays exponentially [50], except the Haar case which is excluded from here on.

Up to now we have used the filter D^j only with $j = J$. The following algorithm accomplishes a wavelet transform by successively coarsening the samples.

ALGORITHM 1. (Wavelet transform).

given samples $\{f(x_{J,i})\}_i$ for some $J \in \mathbb{N}$ with $x_{J,i}$ from (2.10).
Step 1. $f_J(x_{J,i}) = f(x_{J,i})$, set $j = J$.
Step 2. Compute

$$d_{j-1,k} = \sum_n f_j(x_{j,n}) D_{n-2k}^j, \quad k = \cdots \qquad (2.20)$$

Step 3. Subtract the contribution from W_{j-1} at the even grid points

$$f_{j-1}(x_{j-1,i}) = f_j(x_{j,2i}) - \sum_k d_{j-1,k}\psi_{j-1,k}(x_{j-1,i}), \quad i = \cdots \quad (2.21)$$

iterate Step 2 and Step 3 down to $j = 1$.
finally compute $\{c_{0,i}\}_i$ using $\{I_n^0\}_n$ from (2.8).

The algorithm exploits the fact that if f_j is known to belong to V_j, the values at the points $x_{j,i}$ uniquely determine the decomposition in this space by the sampling theorem. These coefficients are computed by the discrete orthogonality relations of Proposition 3. In the periodic case the algorithm even becomes slightly simpler as the final step almost disappears. If, furthermore, the entire set of coeffi-

cients in (2.2) is to be computed, it is more economical to use fast convolution by means of FFT employing the technique described in [22]. But this is not the aim here as we consider nonuniform discretization. Similar to the above algorithm we can now devise an inverse transform by successive recombination using the interpolation property of S and the decomposition according to Proposition 3.

ALGORITHM 2. (Inverse wavelet transform).

given coefficients $\{c_{0,i}\}_i$, $\{d_{j,i}\}_{j=0,...,J-1,i}$.
Step 1. Set $j = 0$ and

$$f_0(x_{0,i}) = \sum_k c_{0,k}\phi_{0,k}(x_{0,i}), \quad i = \cdots \qquad (2.22)$$

Step 2. Compute f_{j+1} at even grid points

$$f_{j+1}(x_{j+1,2i}) = f_j(x_{j,i}) + \sum_k d_{j,k}\psi_{j,k}(x_{j,i}), \quad i = \cdots \quad (2.23)$$

Step 3. Compute f_{j+1} at odd grid points,

$$f_{j+1}(x_{j+1,2i+1}) = \sum_k f_j(x_{j,k}) S_{j,k}(x_{j+1,2i+1})$$
$$+ \sum_k d_{j,k}\psi_{j,k}(x_{j+1,2i+1}), \quad i = \cdots \qquad (2.24)$$

iterate Step 2 and Step 3 for $j = 1, ..., J - 1$.

Using (2.7) and (2.11) Steps 2 and 3 can be assembled in

$$f_{j+1}(x_{j+1,i}) = \sum_k f_j(x_{j,k}) S_{j,k}(x_{j+1,i}) + \sum_k d_{j,k}\psi_{j,k}(x_{j+1,i}), \quad i = \cdots \qquad (2.25)$$

which again makes obvious the role of the cardinal function as a substitute for the scaling function.

In many applications a priori information can be used for adapting the index set of required coefficients in (2.2) to a given function f. In most cases local importance of fine scale coefficients is due to the presence of singularities or almost-singularities in f. The decay of the wavelet coefficients in scale and space depends on the strength of the singularity and is well known; see [27, 37] and others. Then, the relevant indices for $d_{j,i}$ fulfil a so-called cone condition. It roughly means that at a given point x with finest local scale j_x all basis functions on scales $j < j_x$ of which the (numerical) support contains x are retained. This property is no prerequisite for the sequel but increases the efficiency of the method.

Although generally having noncompact support the filters D^j and $\psi_{j,i}$ exhibit rapid decay and can therefore be truncated in space up to some prescribed tolerance. The operations in step 2 and step 3 of Algorithm 1 then are

only carried out on subgrids of $\{x_{j,i}\}_i$. This increases the savings in each step and requires f to be known only at the union of the involved truncated grids. At the price of a slight error, apart from the one due to the neglect of small coefficients, it yields an $O(N)$ operation count, where N is the number of active basis functions with the order constant depending on the (fixed) length of the employed filters. The operation count for the inverse transform is the same as for Algorithm 1 since the sums in (2.24) are shorter than the one in (2.20). Observe that the error from truncation of the filters does not affect the perfect reconstruction property of the transform and its inverse which is preserved by construction. This was not necessarily the case in [22] where, furthermore, a grid finer than $\{x_{j,i}\}_i$ was required for the computation of $\{d_{j-1,i}\}_i$ to avoid aliasing. As a consequence, the restriction to wavelets well localized in Fourier space such as the Meyer wavelets is removed by the present method.

3. OPERATOR-ADAPTED BASES

An essential step is now the extension of Algorithm 1 to biorthogonal vaguelettes. These can be adapted to certain operators so that such an algorithm may be applied to solve (pseudo-) differential or integral equations by a Petrov–Galerkin scheme. The result is a so-called wavelet–vaguelette decomposition of the solution and the right-hand side. Although wavelets are employed to furnish better bases for numerical algorithms than trigonometric polynomials the analysis below relies heavily on the Fourier transform. This technique is well suited for the considered operators and furnishes powerful tools.

Let us denote by $\sigma(\xi) = \sum_{m=0}^{s} a_m (2\pi i \xi)^m$ the symbol of a linear operator L of order $s \in \mathbb{N}_0$ with constant coefficients given by $Lu = \sum_{m=0}^{s} a_m (\partial_x)^m u(x)$. In the following we consider inhomogeneous elliptic differential operators, which means that $\sigma(\xi) > 0$, and we aim to solve the equation

$$Lu = f \tag{3.1}$$

for $u(x)$. The inverse L^{-1} is represented by the symbol $1/\sigma(\xi)$ and the adjoint L^* by the complex conjugate $\overline{\sigma(\xi)}$. The corresponding homogeneous operator which is obtained by only retaining the highest order term of L is denoted $\dot{L}$ with the symbol $\dot{\sigma} = a_s(2\pi i \xi)^s$.

Under suitable conditions (cf. below) one can define the functions

$$\theta_{j,i} = (L^*)^{-1}\psi_{j,i}, \quad \mu_{j,i} = L\psi_{j,i} \tag{3.2}$$

$$\eta_{j,i} = (L^*)^{-1}\phi_{j,i}, \quad \nu_{j,i} = L\phi_{j,i}. \tag{3.3}$$

By construction these fulfill the biorthogonality relations

$$\langle \theta_{j,i}, \mu_{k,m} \rangle = \delta_{j,k}\delta_{i,m}, \quad \langle \eta_{j,i}, \nu_{j,k} \rangle = \delta_{i,k}. \tag{3.4}$$

Observe that scale invariance (2.1) no longer holds. Apart from a scaling factor depending on s the reason is that an inhomogeneous operator (in contrast to a homogeneous one) involves spatial scales on its own determined by the ratios of different coefficients. These ratios are not altered with j in (3.2) and (3.3). The functions $\theta_{j,i}$, $\mu_{j,i}$ are called vaguelettes [37] as they have similar properties as wavelets (not necessarily being orthogonal) apart from dilation invariance. In particular, they have vanishing moments and fast decay which is shown below. The latter property is of primary concern since it affects the length of the involved filters in the proposed method.

We now analyse the functions defined in (3.2) and (3.3), as well as the required operator-adapted cardinal functions. Replacing L with its homogeneous counterpart permits us to verify that for $j \to \infty$, i.e., for strong refinement, no degradation occurs. As $\lim_{j\to\infty} (\|L\psi_{j,i}\|/\|\dot{L}\psi_{j,i}\|) = 1$ for any suitable norm $\|.\|$ the homogeneous operator in some sense constitutes a worst-case limit of L when considering its action on elements of W_j with increasing j.

Let us start with the following statement which can be deduced from classical Fourier analysis [45]. It determines the decay of a function in physical space by the regularity of its Fourier transform.

PROPOSITION 4. *Let*

$$(d_\omega)^k \hat{f} \in L^1(\mathbb{R}), \quad k = 0, ..., n, \tag{3.5}$$

for some $n \in \mathbb{N}_0$. Then $x^n f \in L^\infty(\mathbb{R})$. This yields (Riemann-Lebesgue)

$$\lim_{|x|\to\infty} x^n f = 0. \tag{3.6}$$

A priori, the Fourier transform in (3.5) has to be understood in a distributional sense. However, in all applications below the considered expressions belong to $L^2(\mathbb{R})$ as well (without being mentioned explicitly every time) so that $\hat{f}$ has the classical L^2-meaning. Proposition 4 can now be applied to the functions defined above.

PROPOSITION 5. *Let L be an inhomogeneous elliptic operator of order $s \in \mathbb{N}$ with symbol $\sigma > 0$. Let $\dot{L}$ be the corresponding homogeneous operator containing only the highest order term of L. Consider an MRA with the orthogonal wavelet ψ fulfilling*

$$|d_\omega^k \hat{\psi}(\omega)| \leq \frac{C_k}{(1 + |\omega|)^{r+1+\epsilon}}, \quad k = 0, ..., n; \quad n \in \mathbb{N}_0, \tag{3.7}$$

for some $r \geq s$, $\epsilon > 0$, and positive constants C_k. Suppose further that

$$\int x^l \psi(x)\, dx = 0, \quad l = 0, ..., M, \tag{3.8}$$

with $M \geq s$. Then the functions θ, μ, η, ν as defined in (3.2) and (3.3) (with $\theta = \theta_{0,0}$ etc.) have the same asymptotic decay rate as ϕ and ψ. This remains true for θ, μ, ν when replacing the inhomogeneous operator by the homogeneous one.

Before turning to the proof a few remarks are appropriate. It will become clear that the above assumptions are not necessary conditions for the required decay rates but rather sufficient ones. They are oriented toward the typical MRAs and are well suited for the present examples. For example, an r-regular MRA as defined in [37] is a special case of the considered MRAs and is obtained if (3.5) holds for any $n \in \mathbb{N}_0$. The above setting partly results from the desire to cover Meyer wavelets which need not be r-regular. Let us sum up the different parameters characterizing the MRA: r determines the differentiability of ϕ and ψ, M specifies the number of vanishing moments, and n describes the decay of ϕ, ψ, and their derivatives up to order r. For particular MRAs these parameters are coupled differently. The Meyer MRA corresponds to infinite r and infinite M while n depends on the construction ($n = 4$ in the present computations). Spline wavelets are related to $r = m - 1$, $M = m - 1$ and infinite n, where m denotes the (even) order of the spline.

Proof. Equation (3.7) yields

$$d_\omega^k \hat{\psi}(\omega) \in L^1(\mathbb{R}), \quad k = 0, ..., n. \tag{3.9}$$

Hence from Proposition 4

$$|\psi(x)| \leq \frac{C}{(1 + |x|)^n} \tag{3.10}$$

for some positive C. As the wavelet and the orthogonal scaling function are intimately related by construction, (3.7) and, therefore, (3.10) apply for ϕ as well. Obviously, the power r is not required in the above. It serves, however, to prove the same decay for the derivatives in space $d_x^k \phi$ and $d_x^k \psi$ up to $k = r$, as these are reflected by multiplication with ω^k in Fourier space. Hence, ν and μ which are just sums of derivatives up to order $s \leq r$ decay similarly to (3.10). This is not modified when replacing L with $\dot{L}$. Now consider θ defined by $\hat{\theta} = \hat{\psi}/\overline{\sigma}$. The existence of the derivatives of $\hat{\psi}$ up to $k = n$ and $\sigma \in C^\infty$, $\sigma > 0$ show that $d_\omega^k \hat{\theta}$, $k = 0, ..., n$, exist. For small ω the symbol tends to a constant while $\sigma \sim \omega^s$ for large ω. Hence, if $d_\omega^k \hat{\psi} \in L^1(\mathbb{R})$ so is $d_\omega^k \hat{\theta}$. Application of Proposition 4 shows the decay rate (3.10). The same arguments apply to η. Switching to

the homogeneous operator $\dot{L}$ with symbol $\dot{\sigma}(0) = 0$ may produce a singularity when dividing by the symbol. As $\hat{\phi}(0) = 1$, the function η cannot be constructed in a classical sense. In other words, the equation $\dot{L}\eta = \phi$ cannot be solved for the right-hand side ϕ. This is different for $\dot{L}\mu = \psi$. In Fourier space (3.8) reads

$$d_\omega^l \hat{\psi}(\omega)\big|_{\omega=0} = 0, \quad l = 0, ..., M. \tag{3.11}$$

As $M \geq s$, the expression $\hat{\theta} = \hat{\psi}/\overline{\sigma}$ still vanishes at $\omega = 0$. Therefore $\hat{\theta}$ and its derivatives exist and remain integrable close to the origin also for the homogeneous case. For large ω the situation is the same as before. ∎

Proposition 5 has been formulated for the scale $j = 0$. Due to the rescaling property (2.1) for the functions $\psi_{j,i}$ it holds for all j. Inequality (3.10) is just modified by supplementary factors 2^{js} or 2^{-js} in the constants and rescaling of x by 2^j. Other properties can be deduced immediately by similar reasoning.

COROLLARY 2. *Under the conditions of Proposition 5 it can be shown that ψ, $\phi \in H^r$, μ, $\nu \in H^{r-s}$, and θ, $\eta \in H^{r+s}$ which holds, apart from η, for the homogeneous case as well. Furthermore, θ and μ have $M + 1$ vanishing moments. In the homogeneous case this number modifies to $M + 1 - s$ and $M + 1 + s$, respecively.*

We now turn to the cardinal Lagrange functions in the operator-adapted case and define the spaces

$$V_{L;j} = \overline{\text{span}}\{Lb_{J,i}\}_i = \overline{\text{span}}\{\nu_{J,i}\}_i. \tag{3.12}$$

Cardinal functions of these spaces are obtained similarly as before.

PROPOSITION 6. *Under the conditions of Proposition 5 the spaces $V_{L;J}$ have a cardinal Lagrange function $S_{L;J}$ if*

$$\sum_{k \in \mathbb{Z}} \sigma(\omega + 2^J k)(\hat{b_j})(\omega + 2^J k) \neq 0. \tag{3.13}$$

It is given by

$$\widehat{S_{L;J}}(\omega) = \frac{\sigma(\omega)\hat{b_J}(\omega)}{2^J \sum_{k \in \mathbb{Z}} \sigma(\omega + 2^J k)(\hat{b_J})(\omega + 2^J k)}. \tag{3.14}$$

The same remains true for L replaced by $\dot{L}$.

PROPOSITION 7. *Under the conditions of Proposition 5 the functions S, S_L, and $S_{\dot{L}}$, if they exist, fulfil the same asymptotic decay estimates (3.10) as ϕ and ψ.*

Proof. According to the remark after Proposition 1, $\hat{S}$ can be obtained through dividing $\hat{\phi}$ by $\hat{\phi}^*$, a 1-periodic

function. The condition $|\hat{\phi}^*| \geq C > 0$ has to be fulfilled for S to exist. Hence, $|\hat{S}| \leq (1/C)|\hat{\phi}|$. By construction $\hat{\phi}^*$ has the same number of derivatives as $\hat{\phi}$ so that $\hat{S}$ fulfills the conditions (3.7) and therefore the assertion. $\widehat{S_L}$ is obtained analogously as $\hat{S}$ replacing $\hat{\phi}$ by $\hat{\nu}$. Using Proposition 5 the above remarks apply identically to $\widehat{S_L}$ and $\widehat{S_L}$. ∎

It can be shown that the sets $\{2^{-sj}\mu_{j,i}\}$, $\{2^{sj}\theta_{j,i}\}$, and $\{2^{-sj}\nu_{j,i}\}$ form Riesz bases of the spaces they generate [22, 40]. Considering the homogeneous case we have seen that an algorithm involving the functions $\eta_{j,i}$ would not be practical for large j. Ponenti [40] points out that with increasing j these functions more and more tend to the Greens function of the (inhomogeneous) operator. The common shape for all j destroys the essential zooming-in property. Hence, the functions $\{2^{sj}\eta_{j,i}\}$ do not form a Riesz basis in the limit $j \to \infty$. This important observation triggered the construction in the cited reference where the unknown u in (3.1) is developed in terms of $\theta_{j,i}$ (and not in terms of $\psi_{j,i}$ as below). To avoid the use of the unstable set $\eta_{J,i}$ a modified basis is constructed by means of some finite difference operator compensating the singularity in Fourier space. This makes the construction rather complicated. Furthermore, the projection step depends on this filter and is not obvious.

The present algorithm has been developed independently from [40] and is different in the following sense. We do not assume $u \in H^{r+s}$, as with the representation in terms of $\theta_{j,i}$, but rather $u \in H^r$, and we approximate the unknown u in (3.1) by some $u_J \in V_J$,

$$u_J(x) = \sum_i c_{0,i}\phi_{0,i}(x) + \sum_{j=0}^{J-1}\sum_i d_{j,i}\psi_{j,i}(x). \qquad (3.15)$$

The right-hand side f is then approximated accordingly by $f_{L;J} \in V_{L;J}$ which can be expressed as

$$f_{L;J}(x) = \sum_i \langle f, \eta_{J,i}\rangle \nu_{J,i}(x) = \sum_i \langle f, \eta_{0,i}\rangle \nu_{0,i}(x)$$
$$+ \sum_{j=0}^{J-1}\sum_i \langle f, \theta_{j,i}\rangle \mu_{j,i}(x). \qquad (3.16)$$

Inserting (3.15) and (3.16) in (3.1) and applying a Petrov–Galerkin method with test functions $\{\eta_{0,i}, \theta_{j,i}\}$ shows that, having computed the two rightmost terms of (3.16), the solution u_J is obtained with $c_{0,i} = \langle f, \eta_{0,i}\rangle$, $d_{j,i} = \langle f, \theta_{j,i}\rangle$ in (3.15). In order to determine these coefficients we use the representation of $f_{L;J}$ in terms of the cardinal Lagrange function $S_{L;J}$ of $V_{L;J}$ analogously to (2.6)

$$f_{L;J}(x) = \sum_i f\left(\frac{i}{2^J}\right) S_{L;J}\left(x - \frac{i}{2^J}\right). \qquad (3.17)$$

The task then is to accomplish a basis transform from $\{S_{L;J,i}\}$ to $\{\nu_{0,i}, \mu_{j,i}\}$ when f is given at the required grid points. Due to Proposition 7, the limit $j \to \infty$ does not constitute a problem in the construction. Of course, the sums of $\phi_{0,i}$ and $\nu_{0,i}$ in (3.15) and (3.16) can be replaced by linear combinations of $S_{0,i}$ and $S_{L;0,i}$, respectively. This avoids another type of filters.

The biorthogonal basis is now used in the adaptive algorithm of the previous section, replacing $S_{J,m}$ with $S_{L;J,m}$ and D^j_m with

$$D^j_{L;m} = \langle S_{L;j,m}, \theta_{j-1,0}\rangle. \qquad (3.18)$$

This filter fulfills analogous relations as D^j apart from scale invariance, in particular discrete orthogonality and vanishing moments. Its decay is determined by Propositions 5 and 7. Another reasoning is illustrative and more direct. It uses the equivalent of Proposition 4 for the Fourier transform $\hat{f}^*(\omega)$, $\omega \in \mathbb{T}$ (see Appendix).

PROPOSITION 8. *Under the conditions of Proposition 6 the filter $D^j_{L;m}$ has the same decay with m as D^j_m.*

Proof. Inserting (3.14) and the definition of $\theta_{j,i}$ (3.2) into (3.18) leads to cancellation of the symbol σ and

$$D^j_{L;m} = \int_{\mathbb{T}} \frac{\widehat{b_{j,0}}(\omega)\,\overline{\widehat{\psi_{j-1,0}}(\omega)}\,e^{-2\pi i m\omega}}{2^J \sum_{k\in\mathbb{Z}} \sigma(\omega + 2^J k)(\widehat{b_J})(\omega + 2^J k)}\,d\omega. \qquad (3.19)$$

The denominator is a smooth nonzero bounded 2π-periodic function which does not alter the decay properties in physical space. In [37] a similar argument is applied to the orthonormalization procedure for the classical wavelets. ∎

The actual computation of $D^j_{L;m}$ is not based on (3.19) but is described in Section 4. We now obtain the following algorithm for the adaptive solution of (3.1).

ALGORITHM 3. (Operator-adapted decomposition).

given index set $\Lambda_d \subset \Lambda_J = \{(j, i) | j = 0, ..., J - 1, i \in \mathbb{Z}\}$ for the amplitudes $d_{j,i}$ of a lacunary wavelet basis in V_J with some $J \in \mathbb{N}_0$, a method to evaluate f.

Step 0. Compute D^j_L, $\mu_{j-1,0}$ $j = 1, ..., J$, where $J - 1$ is the finest scale in Λ_d. Truncate these in space according to a given precision.

Step 1. Determine the index set Λ_x of points $x_{j,i}$ required in the subsequent quadratures. Require the r.h.s. at these points

$$f_J(x_{j,i}) = f(x_{j,i}), \quad (j, i) \in \Lambda_x. \qquad (3.20)$$

Set $j = J$.

Step 2.

$$d_{j-1,k} = \sum_{(j,i)\in\Lambda_x} f_j(x_{j,i}) D^j_{L;i-2k}, (j-1,k) \in \Lambda_d. \quad (3.21)$$

Step 3.

$$f_{j-1}(x_{j-1,i}) = f_j(x_{j,2i}) - \sum_{(j-1,k)\in\Lambda_d} d_{j-1,k}\mu_{j-1,k}(x_{j-1,i}),$$
$$(j-1,i) \in \Lambda_x. \quad (3.22)$$

iterate Step 2 and step 3 down to $j = 1$.
final step compute

$$c_{0,k} = \sum_i f_0(x_{0,i})I^0_{L;k-i} \quad (3.23)$$

with $I^j_{L;n} = \langle S_{L;j,n}, \eta_{j,0} \rangle$, analogous to (2.8).

In short, the proposed algorithm for the solution of an ODE (3.1) reads as follows: given the values of the r.h.s. at an appropriate set of points, Algorithm 3 is employed to determine the coefficients in the development (3.15) of the solution u. The value of the solution at a point of the grid is then obtained by Algorithm 2. Hence, we employ a vaguelette-decomposition and a wavelet-reconstruction to solve (3.1). This algorithm has been implemented in a periodized version which is discussed in the following section. Observe that when the filters applied in both steps are not truncated and the entire set of basis functions is used, the method is exactly equivalent to a collocation algorithm on the grid $\{x_{J,i}\}_i$. The inversion of a linear system is replaced by the application of filters into which the inverse of the operator has been incorporated. As soon as these are truncated this yields a method which is neither a Galerkin nor a collocation method but a hybrid one. It relies on both, the localization in space and frequency, as well as the orthogonality of the wavelets.

4. TRANSITION TO PERIODIC MULTIRESOLUTIONS AND IMPLEMENTATION

The computations below have been executed under periodic conditions. This section therefore gives a comprehensive understanding of what sometimes is just subsumed by the term periodization. We furthermore detail the practical computation of the employed filters.

Starting from an MRA on the real line, an MRA on the circle $\mathbb{T}$ can be constructed through the projection

$$\tilde{f}(x) = \sum_{n\in\mathbb{Z}} f(x+n) \quad (4.1)$$

from $L^2(\mathbb{R})$ onto $L^2(\mathbb{T})$ [38, 37]. In Fourier space it reads

$$\hat{\tilde{f}}(n) = \hat{f}(n), \quad n \in \mathbb{Z} \quad (4.2)$$

(see Appendix). This generates the periodic analogues $\widetilde{b_{j,k}}$, $\widetilde{\phi_{j,k}}$, $\widetilde{\psi_{j,k}}$ of the functions $b_{j,k}$, $\phi_{j,k}$, $\psi_{j,k}$ and the periodic MRA of the spaces $\widetilde{V_j} = \text{span} \{b_{ji}\}_{i=0,...,2^j-1}$, $j \in \mathbb{N}_0$. The index range is due to the periodicity $\widetilde{f_{j,i}} = \widetilde{f_{j,i+k2^j}}$ $(k \in \mathbb{Z})$ introduced by (4.1). It carries over to all filters and functions in $L^2(\mathbb{T})$ below. By construction the orthogonality between shift invariant functions is preserved under (4.1). Furthermore, $\widetilde{\phi_{j,k}} = 1$ for $j \leq 0$ as the functions $\{\phi_{j,i}\}_i$ constitute a partition of unity, and $\widetilde{S_{0,0}} = \widetilde{\phi_{0,0}}$ for the same reason. Denoting this function by $\widetilde{\psi_{-1,0}}$ for brevity, any $\widetilde{f_J} \in \widetilde{V_J}$ can then be written as

$$\widetilde{f_J}(x) = \sum_{j=-1}^{J-1} \sum_{k=0}^{\lceil 2^j-1 \rceil} d_{j,k}\widetilde{\psi_{j,k}}(x). \quad (4.3)$$

In the periodic setting the indices in scale no longer refer to an affine transform such as (2.1) but rather to applying (2.1) for the nonperiodic counterpart followed by (4.1). A result is that functions and filters are related through recurrence relations in Fourier space [38]. In other words, their Fourier transforms are obtained from the nonperiodic counterparts through coarser and coarser sampling for decreasing j. The values of $\widetilde{H^j_n} = \langle \widetilde{\phi_{j,n}}, \widetilde{\phi_{j-1,0}} \rangle$, $n = 0, ..., 2^j - 1$, for example, can be obtained by

$$\widehat{(\widetilde{H^j})_k} = 2^{-j}\hat{H}^*\left(\frac{k}{2^j}\right), \quad k = 0, ..., 2^j - 1, \quad (4.4)$$

with $\hat{H}^*$ from (2.4). Using the mapping (4.1) a cardinal Lagrange function is readily obtained similarly to Proposition 1.

PROPOSITION 9. *Let b fulfil the requirements of Proposition 1 and let* $\widetilde{V_J} = \text{span}\{\widetilde{b_{j,i}}\}_{i=0,...,2^j-1}$ $(j \in \mathbb{N}_0)$ *be defined through* (2.1), (4.1). *Then a cardinal Lagrange function of* $\widetilde{V_J}$ *exists and is given by*

$$\widehat{\widetilde{S_j}}(n) = \frac{\widehat{\widetilde{b_j}}(n)}{2^j\widehat{(\widetilde{b_j})}_n}, \quad n \in \mathbb{Z}. \quad (4.5)$$

Proof. Since V_j is spanned by shifts of S_j, $\widetilde{V_j}$ is spanned by shifts of $\sum_{k\in\mathbb{Z}} S_j(x+k)$. Obviously, the interpolation property is preserved through periodization so that this sum indeed is again a cardinal Lagrange function of $\widetilde{V_j}$ and therefore defines $\widetilde{S_j}$ due to its uniqueness. Using (2.9), (4.2), and (A.4) yields (4.5). The nonvanishing denominator is ensured by the condition on b. ∎

The required filters in the algorithms devised above have to be determined in a preprocessing step. Throughout, we first compute the exact values and only subsequently truncate the filters with respect to their length. We employ

multiresolutions of Battle–Lemarié spline wavelets of even order and Meyer wavelets. As both have noncompact support, a few remarks are appropriate.

In the present cases the filters H, G, I, D, I_L, D_L for the nonperiodic MRAs are given explicitly in Fourier space. Recall that these expressions are 1-periodic functions in ω (cf. Equation (2.4)). Hence, no error is introduced through the periodization by replacing ω with $k/2^j$. This property is not shared by the functions ϕ, ψ, S, μ, etc.; they can be defined in Fourier space but have large or unbounded support in ω. Therefore the exact values of these functions have to be deduced from the filters. The values $\widetilde{\psi_{J-1,0}}(x_{J,i})$, for example, are computed by an inverse wavelet transform [38] having initialized with $d_{j,i} = \delta_{j,J-1}\,\delta_{i,0}$. In the particular case of Meyer wavelets the compact support in Fourier space can be used to alternatively obtain the function's values by a DFT of appropriate length since the sum in (A.6) contains at most two entries. As the symbol σ does not alter the compact support in frequency space this holds for $\tilde{\theta}, \tilde{\mu}, \widetilde{S_L}$ as well.

For spline wavelets the procedure is more involved. We first compute an interpolation function in the nonperiodic case. Thereto, $b = N_m$ with N_m designating the B-spline of mth order; hence, $Lb_j = 2^{j/2}\, LN_m(2^j x)$. Relating $\widehat{N_m}^*$ to the derivative of the cotangent function [13], formulae for $\widehat{Lb_j}^*$ are deduced to express $\widehat{S_{L;j}}(\omega)$. Analogously to Eq. (2.8) this defines the operator adapted interpolation filter $\widehat{I_L^j}^*(\omega) = \widehat{S_{L;j}}(\omega)/\widehat{\nu_j}(\omega)$.

Due to the linearity of the operator L the functions μ, ν fulfil the same refinement equation as ψ, ϕ. Hence, $\widehat{G_L^j}^* = \widehat{G^j}^*$. This is used to compute the function

$$\widehat{D_L^j}^*(\omega) = \widehat{G_L^j}^*(\omega)\,\overline{\widehat{I_L^j}^*(\omega)} \tag{4.6}$$

which is then sampled to accomplish the transfer to the periodic setting. Subsequently, the values of $\widetilde{\mu_{j,0}}$ at grid points are generated by the filters as described above.

Finally note that different MRAs can, of course, be used to start from. However, we conjecture that a construction in which all the required filters are of compact support cannot be obtained. Daubechies wavelets, for example, have compact support, but the related cardinal function has not [50]. The construction of interpolating orthogonal scaling functions ($\phi = S$) with compact support is impossible [17]. Such functions can only be obtained by relaxing the requirement of compact support to exponential decay [32, 14]. Another class of interpolatory MRAs with compactly supported functions can be generated by the correlation function of biorthogonal scaling functions [24]. Special cases are the fundamental functions of Lagrange iterative interpolation [19] which is equivalent to the Daubechies autocorrelation function [17] used, e.g., in [20, 5]. Since for these interpolatory MRAs "wavelets" are generally

defined by $\psi(x) = \phi(2x - 1)$, fast interpolatory transforms exist, also, in the adaptive case [4]. However, these functions, ψ, do not have vanishing moments and are nonorthogonal, so that they cannot be used in the present approach. Also the construction of compactly supported operator-adapted wavelets in [15] does not lead to full (bi-)orthogonality of the basis. Further research is required on this topic.

5. TWO-DIMENSIONAL ADAPTIVE ALGORITHM

We now extend the present method to tensor product MRAs defined in [37]. In this framework the solution u is developed as

$$u_J(x, y) = \sum_{k_x}\sum_{k_y} c_{0,k_x,k_y}\,\phi_{0,k_x,k_y}(x, y)$$
$$+ \sum_{j=0}^{J-1}\sum_{k_x}\sum_{k_y}\sum_{\epsilon=1}^{3} d_{j,k_x,k_y}^{\epsilon}\,\psi_{j,k_x,k_y}^{\epsilon}(x, y) \tag{5.1}$$

with

$$\phi_{j,k_x,k_y}(x, y) = \phi_{j,k_x}(x)\,\phi_{j,k_y}(y) \tag{5.2}$$

and

$$\psi_{j,k_x,k_y}^{\epsilon}(x, y) = \begin{cases} \psi_{j,k_x}(x)\,\phi_{j,k_y}(y), & \epsilon = 1, \\ \phi_{j,k_x}(x)\,\psi_{j,k_y}(y), & \epsilon = 2, \\ \psi_{j,k_x}(x)\,\psi_{j,k_y}(y), & \epsilon = 3. \end{cases} \tag{5.3}$$

The method previously described for the solution of an ODE in space can now be applied analogously to the discretization of a PDE in two dimensions. The symbol then depends on two coordinates; i.e., $\sigma = \sigma(\xi_x, \xi_y)$. Since it can not generally be decomposed as $\sigma_x(\xi_x)\sigma_y(\xi_y)$, the resulting operator-adapted cardinal function, vaguelettes, and filters are truely two-dimensional and do not exhibit a structure analogous to (5.2) or (5.3). (An ADI time discretization would yield such an operator at the price of altering fine-scale components of the solution.) Nevertheless, similar decay in space as proved above can be shown for the two-dimensional case using the same techniques. Periodicity is accounted for by the technique of Section 4.

6. NUMERICAL EXPERIMENTS

As a preliminary step the precision of the wavelet transform defined in Section 2 has been investigated for different truncations. Setting $f = \psi_{j,0}$ ($j = -1, ..., J - 1$), all coefficients are computed up to $J - 1$. The left part of Table I reports the quantity

TABLE I

Projection Error E_1 of Algorithm 1 and E_2 of Algorithm 2 for Meyer Wavelets, Cubic Spline Wavelets ($m = 4$), and Quintic Spline Wavelets ($m = 6$)

	E_1			E_2		
K	Meyer	$m = 6$	$m = 4$	Meyer	$m = 6$	$m = 4$
Full grid	8.7 E-14	5.7 E-14	3.4 E-14	5.5 E-14	7.7 E-14	5.7 E-14
40	2.7 E-5	3.8 E-5	5.6 E-7	8.9 E-6	1.4 E-5	2.2 E-7
30	1.6 E-4	4.1 E-4	1.8 E-5	9.1 E-5	1.2 E-4	5.7 E-6
20	8.6 E-4	4.5 E-3	5.3 E-4	6.3 E-4	1.2 E-3	1.6 E-4

Note. K denotes the number of points from the center of D^j, S_j, and $\psi_{j,i}$ at which summations are stopped, respectively. Finest scale is $J = 10$.

$$E_1 = \max_{j,k,m}\{|\langle\psi_{j,0},\psi_{k,m}\rangle_Q - \delta_{j,k}\,\delta_{0,m}|\}, \qquad (6.1)$$

where the index Q of the scalar product denotes its evaluation by the described recursive quadrature of Algorithm 1. In an analogous way the inverse transform has been tested. The error E_2 is defined similarly to (6.1), replacing $\psi_{j,0}$ with the function generated by the inverse transform and $\langle \cdot\,,\,\cdot\rangle_Q$ by the exact scalar product. This is realized in starting from $d_{j,0} = 1$ for one particular value of j and all other coefficients zero. An inverse transform with truncation and a subsequent exact forward transform without truncation are then executed.

A practically relevant example for the presented method is a Helmholtz-type equation arising, e.g., from a semi-implicit time discretization of parabolic equations as applied below. Hence, we set

$$L = \lambda - \partial_{xx}, \quad \lambda \in \mathbb{R}^{>0}; \qquad (6.2)$$

i.e., $\sigma(\xi) = \lambda + 4\pi^2\xi^2$, $s = 2$. In the sample computations $\lambda = 150$ has been used corresponding to the time stepping for the PDE below.

Similar to Table I we first consider the influence of the truncation on the orthogonality of the basis functions in the operator-adapted case. Some examples are assembled in Table II. The error E_3 is defined as in (6.1) replacing $\psi_{j,0}$ by $\mu_{j,0}$ and $\psi_{k,m}$ by $\theta_{k,m}$ (unfortunately, comparison to a similar table in [22] is not possible for implementational reasons). The level of round-off errors is given by the first line. The precision achieved with truncated filters increases if these have stronger decay, i.e., in case of low regularity of the basis. The observed behavior is related to the filters D_L plotted in Fig. 1. According to Proposition 8 their (algebraic) decay is the same as the decay of D which is determined by the properties of the MRA. Indeed, Fig. 1 shows exponential decay when employing spline wavelets and algebraic decay for Meyer wavelets.

Next, we report the precision obtained for the solution

of the Helmholtz equation (3.1), (6.2), with a right-hand side such that the exact solution is

$$u_{ex} = e^{-\gamma^2(x-1/2)^2}, \quad \gamma^2 = 16000. \qquad (6.3)$$

Figure 2 displays the resulting L^2-approximation error when computing all wavelet amplitudes of the solution, the L^∞-error behaves analogously. As stated before, the use of untruncated filters results in a pure collocation method the convergence rate of which is determined by the regularity of the basis functions. With truncated filters the approximation cannot be improved beyond the level induced by the defect in orthogonality. Hence, the error tends to a constant with increasing J when this level is reached. Observe that the values in Fig. 2 nicely correspond to those of Table II (in general a multiplicative factor appears). Furthermore, the result with Meyer wavelets can be compared to Fig. 7 of [22]. A decrease of the error by about two orders of magnitude or, in other terms, half the

TABLE II

Projection Error E_3 of Algorithm 3 for Meyer Wavelets and Quintic and Cubic Spline Wavelets

| K_D, K_μ	Meyer	$m = 6$	$m = 4$
Full grid	1.5 E-12	2.8 E-12	3.5 E-12
60, 60	3.5 E-5	1.1 E-5	3.0 E-8
40, 40	3.5 E-4	8.5 E-4	2.2 E-5
30, 30	1.6 E-3	8.9 E-3	6.1 E-4
80, 60	1.6 E-5	7.7 E-7	2.6 E-9
40, 30	3.4 E-4	1.1 E-3	5.3 E-5

Note. K_D, K_μ denote the number of points from the center of $D_{L,j}$ and $\mu_{j,i}$ at which quadrature and summation are stopped, respectively. Finest scale is $J = 10$.
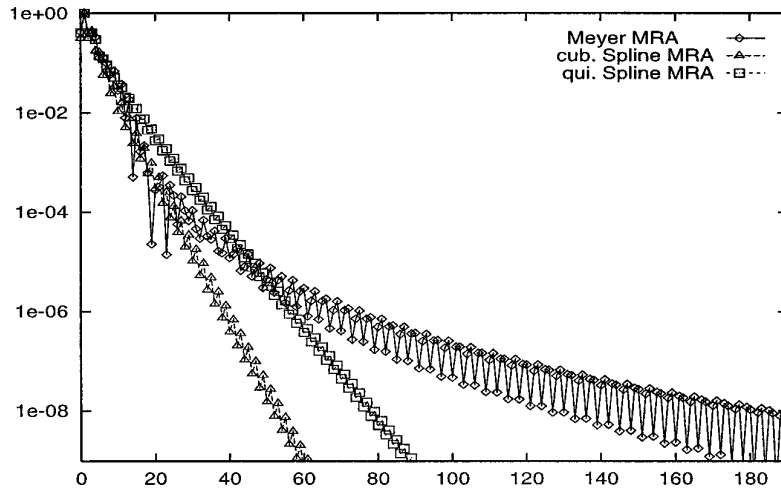
FIG. 1. Absolute value of the filter $D^j_{L,m}$ defined in (3.18) divided by its maximum value versus m for the case of a Meyer MRA, a cubic spline MRA, and a quintic spline MRA with $j = 9$ and L from (6.2). For reasons of symmetry only half of the filter is represented.

filter size for the same precision is observed. Due to the interpolatory approach it is also possible now to use spline wavelets in the solution procedure. The results in the right part of Fig. 2 support the above interpretation: for $m = 6$ only the stronger truncation influences the accuracy, whereas with $m = 4$ the filters could still be shortened without losing considerable precision with respect to the exact result on the respective grids. To assess the amount of adaptivity which is possible by the approach, Table III displays the number N_ϵ of coefficients which are larger in absolute value than the truncation error $\epsilon = \|u - u_{ex}\|_2$ with the full basis depicted in Fig. 2. Employing only these coefficients in an adaptive computation would lead to drastic savings at the expense of an $O(\epsilon)$-error.
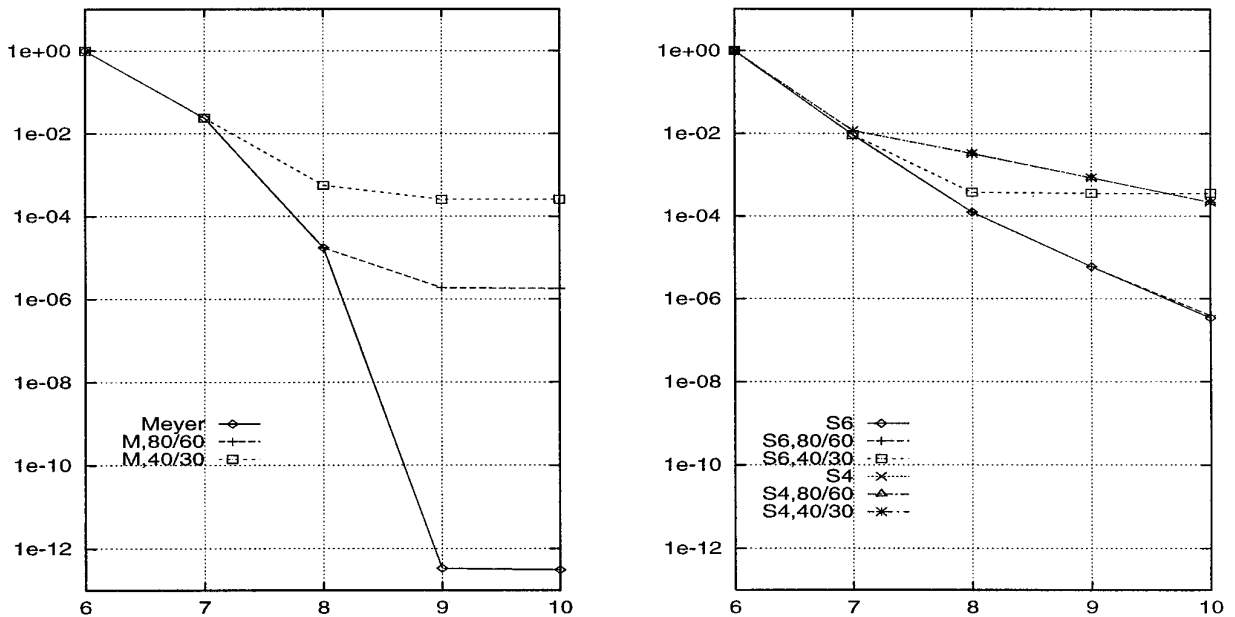
FIG. 2. L^2-error $\|u - u_{ex}\|_2$ versus J for the one-dimensional Helmholtz problem solved with Algorithm 3 and different basic multiresolutions. Left: Meyer wavelets. Right: cubic and quintic spline wavelets (all curves of the former are virtually identical).

TABLE III

Number of N_ϵ of Significant Amplitudes in the Computations of Fig. 2 (see text)

J	7	8	9	10
M full	18	98	508	508
M 80,60	18	98	146	146
M 40,30	18	56	66	66
S6 full	18	74	116	148
S6 80,60	18	74	116	148
S6 40,30	18	56	58	58
S4 full	12	26	38	58
S4 80,60	12	26	38	58
S4 40,30	12	26	38	58

Similar tests have also been made for a two-dimensional Helmholtz problem with ∂_{xx} in (6.2) replaced by $\partial_{xx} + \partial_{yy}$ so that the symbol is $\sigma(\xi_x, \xi_y) = \lambda + 4\,\pi^2(\xi_x^2 + \xi_y^2)$. The imposed exact solution was (6.3) with $(x - \frac{1}{2})^2$ replaced by $(x - \frac{1}{2})^2 + (y - \frac{1}{2})^2$. The employed filters have been truncated in the form of a square. Different forms could perhaps slightly improve the efficiency. The results are qualitatively the same as those reported above, so that we restrict ourselves to the case of cubic spline wavelets here. Table IV displays the obtained L^2-error for different truncations. The number N_ϵ of amplitudes larger than $\epsilon = \|u - u_{ex}\|_2$ was 20, 40, 148 for $J = 7$, $J = 8$, and $J = 9$, respectively, except for the shortest filter where we counted 20, 45, and 112. Since, e.g., for $J = 9$ uniform discretization yields 262,144 degrees of freedom, this illustrates the increased potential for savings through adaptivity in the two-dimensional case which of course depends on the actual solution.

The actual choice of the employed MRA has to depend on the convergence rate in the nontruncated case and the size of the filters which is needed to maintain the required precision. On one hand, there are very regular basis functions and longer filters leading to higher precision on large

TABLE IV

L^2-Error of the Two-Dimensional Helmholtz Problem with Square Truncation of the Fitlers

K_D, K_μ	$J = 7$	$J = 8$	$J = 9$
Full grid	1.0575 E-3	4.1054 E-4	1.0794 E-4
80, 60	1.0575 E-3	4.1054 E-4	1.0794 E-4
40, 30	1.0575 E-3	4.1054 E-4	1.0796 E-4
30, 20	1.0563 E-3	4.1714 E-4	1.3349 E-4

scales. On the other hand, there are bases with low regularity which lead to shorter filters but steeper cones in the index space around singularities or almost-singularities of the solution. Another relation can be drawn to the method of "approximate approximation" proposed by Maz'ya [36]. He considers approximation schemes exhibiting convergence only down to some threshold for the error and, by construction, not below. This exactly corresponds to the saturation observed in this section for truncated filters.

7. ADAPTIVE COMPUTATION OF FLAMES

The above discretization has been devised for the adaptive solution of a PDE with evaluation of the nonlinear terms in physical space. In this section we report results of one- and two-dimensional computations of this type and detail further features of the algorithm.

We consider a reaction–diffusion equation originating from combustion modeling. It describes the propagation of a laminar flame in a quiescent premixed atmosphere and is discussed, e.g., in [10]. For a unitary Lewis number (the ratio of the diffusivity of species to the diffusivity of heat), one-step kinetics, and appropriate initial and boundary conditions the resulting equation for the dimensionless reduced temperature T reads

$$\partial_t T - \nabla^2 T = r(T)$$
$$r(T) = \frac{\beta^2}{2}(1 - T)\,e^{\beta(T-1)/(1+\alpha(T-1))}. \tag{7.1}$$

The variables are scaled such that r unit distance corresponds to the characteristic scale for temperature variations in the flame front. The strong stiffness of this problem results from the fact that this length is typically much smaller than the domain of interest and that, furthermore, the region where $r >> 0$ is only of size $O(\beta^{-1})$ in these units. In all computations we employ the semi-implicit time scheme of second order,

$$\frac{3}{2\Delta t}T^{n+1} - \nabla^2 T^{n+1} = \frac{2}{\Delta t}T^n - \frac{1}{2\Delta t}T^{n-1} + r(2T^n - T^{n-1}), \tag{7.2}$$

where the index n represents the time level and Δt the time step. At this occasion we observe that the implicit discretization of the Laplacian is applied for reasons of stability. If, e.g., the second-order term contains a variable coefficient it can be decomposed into a sum of a constant coefficient operator discretized implicitly and a perturbation discretized explicitly in time. This may in some cases yield the required stability. Another solution is to apply
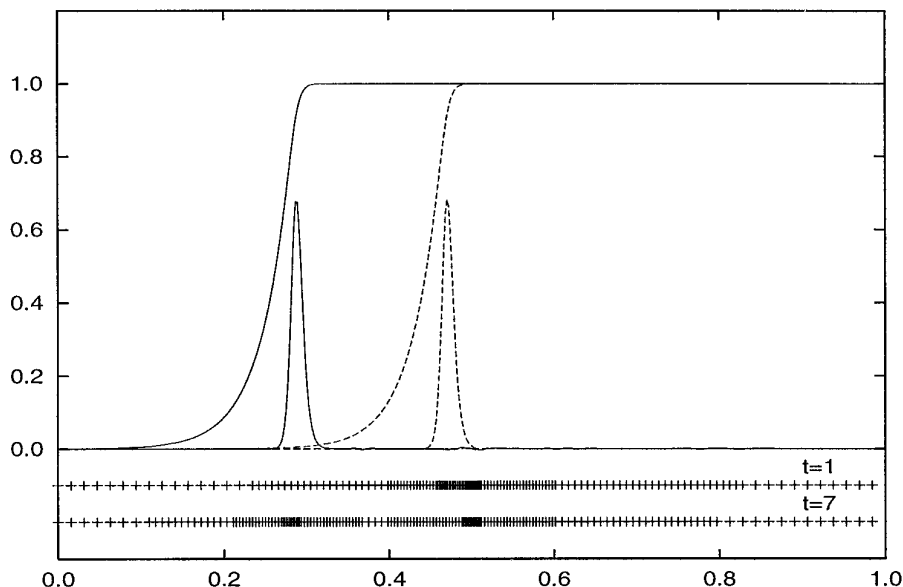
FIG. 3. Temperature $T = \tilde{T} + s$ and reaction rate ω (divided by 2.5 for presentation) versus x for a left-traveling thermodiffusive flame front. The dotted curves correspond to $t = 1$, the continuous ones to $t = 7$. The tics below indicate the centers of the adaptively selected wavelet basis functions computed at the respective times. Their number is larger than the value of N_ϵ mentioned in the text due to the adding of neighbors in scale space. The second cloud for $t = 7$ at $x = 0.5$ is generated by the periodizing function $s(x)$.

the present algorithm with locally constant coefficients in an iterative scheme as investigated in [30] for uniform discretization.

For the one-dimensional computations we consider a steadily propagating flame front similar to the one in [22]. The computational domain $[-L_x/2, L_x/2]$ is mapped onto $[0, 1]$ and a flame is initialized in its middle. For physical reasons the temperature remains constant in a large partition of the domain before and after the front (cf. Fig. 3). The values $T = 0$ and $T = 1$ are attained with the present scaling. Strictly speaking, these values should be imposed as boundary conditions at ∞ and $-\infty$, but for large L_x they can as well be imposed at $x = 0$ and $x = 1$, respectively. As long as the front remains sufficiently far from the boundaries it is useful to consider the quantity $\tilde{T} = T - s$, where s is a smooth function of x with $s(0) = 0$, $s(1) = 1$, and all its derivatives vanishing at $x = 0$ and $x = 1$. Then, $\tilde{T}$ can very well be approximated by a periodic function [18]. (A moving reference frame may be used to generate a steady solution but is avoided here for simplicity.) We employ
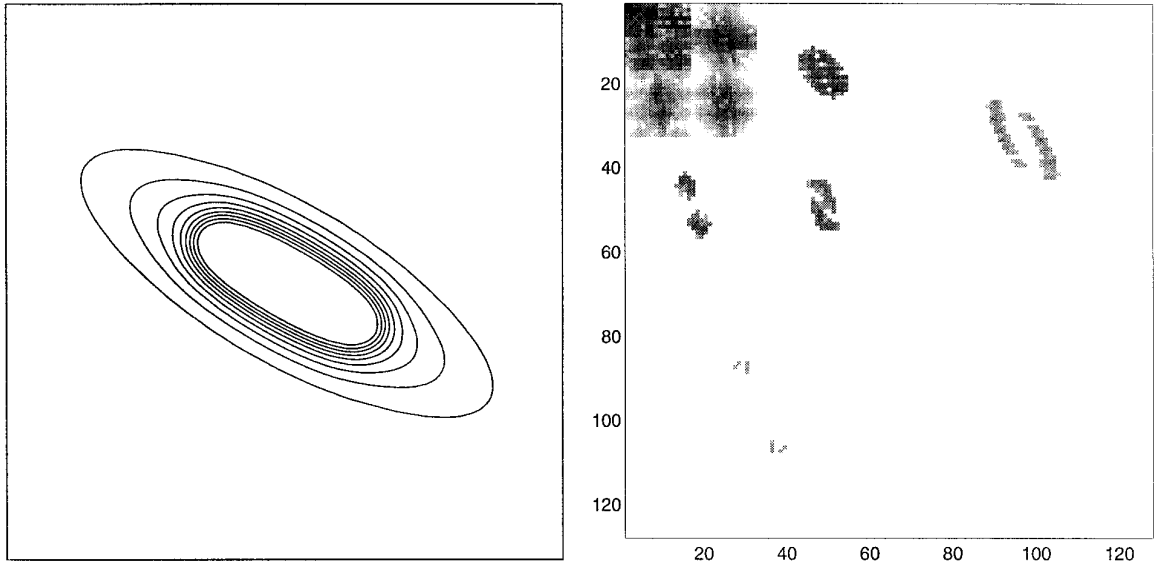
$$s(x) = \tfrac{1}{2}\left(1 + \tanh\left(\tau \tan\left(\pi \times \frac{\pi}{2}\right)\right)\right). \qquad (7.3)$$

from [18] with $\tau = 5$. At each time step the solution is developed in a wavelet sum

$$\tilde{T}^{n+1}(x) = \sum_{(j,i)\in\Lambda_d^{n+1}} d_{j,i}^{n+1} \psi_{j,i}(x). \qquad (7.4)$$

The index set Λ_d^{n+1} is determined from $\tilde{T}^n$ by retaining only those coefficients which are larger than some tolerance ϵ. A moving solution is accounted for by adding to each index (j, i) of this set its neighboring indices $(j - 1, \lfloor i/2 \rfloor)$, $(j, i \pm 1)$, $(j + 1, 2i)$ (if these are not yet present) which then gives Λ_d^{n+1}. The solution is advanced in time by first performing a backward transform of the old solution to the locally refined grid of quadrature points (Algorithm 2). The r.h.s. is then evaluated at these points. Finally, the decomposition into the operator-adapted basis (Algorithm 3) is applied to determine the wavelet amplitudes in (7.4). A result is reported in Fig. 3. This computation for $L_x = 30$, $\alpha = 0.8$, $\beta = 10$ has been performed with cubic spline wavelets and $\Delta t = 0.01$, $J = 10$, $\epsilon = 10^{-5}$. The adaptive discretization follows the front without a problem, requiring a number of significant coefficients of about $N_\epsilon = 66$, most of the time. Nevertheless, the very sensitive reaction rate is well approximated. With respect to former computations [22] the new projection method leads to reduced cpu time (factor of about 4 for this particular setting) and a reduced number of quadrature points. This is particularly advantageous when the evaluation of the r.h.s. is costly.

Let us now solve (7.1) in its two-dimensional form. We

FIG. 4. Computation of an elliptic two-dimensional flame front. Left: level lines of the temperature at $t = 1$. Right: active coefficients in (5.1) located according to (7.5).

avoid the need for periodization here by considering an outward burning flame which, up to a certain time, can be well approximated with periodic boundary conditions. For small Lewis number and additional radiative heat loss such flames exhibit interesting behavior [42] and have been computed in [8]. The computational domain $[-L_x/2, L_x/2]^2$ is mapped onto $[0, 1]^2$ and at each time step the solution is developed according to (5.1) with a lacunary index set. An analogous sequence of computations as in the one-dimensional case is then applied to determine the adaptive wavelet representation of $T^{n+1}(x, y)$. For the neighborhood in scale space of each coefficient (j, i_x, i_y, ϵ) we consider the points $(j \pm 1, i_x, i_y, \epsilon)$, $(j, i_x \pm 1, i_y \pm 1, \epsilon)$, and $(j, i_x, i_y, \mathrm{mod}(\epsilon \pm 1, 3) + 1)$.

Figure 4 reports a result obtained by the presented two-dimensional adaptive wavelet discretization. We used $L_x = 30$, $\Delta t = 10^{-2}$, and $\epsilon = 10^{-5}$. The initial state is given by an inclined elliptical flame front which then propagates in an outward direction. Due to the physical stability of thermodiffusive flames at unitary Lewis number [44] the front relaxes to a circle. This example has been selected as its solution and is difficult to resolve, e.g., by parametrized mapping techniques.

The left part of Fig. 4 shows level lines of the solution at $t = 1$. The right part presents the instantaneous set of adaptively selected coefficients in (5.1). These are represented in the standard way [17, p. 315]; a coefficient d_{j,k_x,k_y}^{ϵ} is positioned at

$$X = 2^j(1 - \delta_{\epsilon,2}) + k_x, \quad Y = 2^j(1 - \delta_{\epsilon,1}) + k_y \quad (7.5)$$

with the origin in the upper left corner and the Y-axis directed downwards. As in the one-dimensional case only the selected degrees of freedom are computed while the remaining ones are set to zero. The finest scale in this computation was $J = 7$, yielding 128×128 possible degrees of freedom. At $t = 1$ only 1510, i.e., roughly 10% of them, are required to represent the solution with the desired accuracy. The employed MRA is based on cubic splines. Observe that, although the basis functions reflect to some extent the orthogonal coordinate system, this does not degrade the adaptive discretization in oblique directions.

8. CONCLUSION

The present algorithm is a step towards an atom-like use of wavelet basis functions for the solution of PDEs. We have developed the method in one dimension and have analyzed the resulting filters. The approach has also been extended to a truly two-dimensional fully adaptive wavelet discretization in space. With respect to earlier work [22] the improved methodology results in a clearer presentation, an easier analysis, and increased efficiency.

The presented method has been implemented for periodic MRAs and could as well be used for initial value problems in unbounded domains. The direct incorporation of essential boundary conditions is not compatible with the approach since it would destroy the shift invariance of the basis. However, the fictitious domain method reduces the solution of such a boundary value problem to the solution of one or more periodic problems. Hence, employing

the proposed adaptive algorithm in this framework will allow us to account for boundary conditions and general domains. See, e.g., [41] for the use with a regular discretization in terms of the scaling function.

It is evident that the filters applied in the construction are still unsatisfactory as they do not have compact support right from the start and have to be truncated. The basic multiresolutions with noncompactly supported cardinal functions are not the only reason for this fact. A further difficulty results from the incorporation of the operator inverse which is related to the Greens function. Its advantage is that no linear system needs to be solved. Other approaches in the literature such as [6, 12] start from the representation of the inverse of an operator by means of a wavelet basis (standard or nonstandard form) and determine an approximation by cancelling small matrix entries. This operation is similar to the employed truncation of filters. Hence, the requirement of truncation is no particularity of the present construction but rather a general feature which, nevertheless, would be convenient to overcome. Future research will be concerned with the construction of improved bases for the presented algorithm and its application to the simulation of turbulence [23].

APPENDIX: DEFINITION OF THE EMPLOYED FOURIER TRANSFORMS

The employed Fourier transforms of square integrable functions are

$$\hat{f}(\omega) = \int_{\mathbb{R}} f(x) e^{-2\pi i \omega x} \, dx, \quad \omega \in \mathbb{R}, \qquad (A.1)$$

$$\hat{\tilde{f}}(n) = \int_{\mathbb{T}} \hat{f}(x) e^{-2\pi i n x} \, dx, \quad n \in \mathbb{Z}, \qquad (A.2)$$

in the nonperiodic case and the periodic case, respectively. The symbol $\mathbb{T}$ designates the circle or one-dimensional torus $\mathbb{T} = \mathbb{R}/\mathbb{Z}$. The brackets around $n \in \mathbb{Z}$ in (A.2) are motivated by (4.2). They serve to distinguish (A.2) from the discrete Fourier transform (DFT) of length 2^j with some $j \in \mathbb{N}_0$ defined by

$$\hat{\tilde{f}} = \frac{1}{2^j} \sum_{n=0}^{2^j-1} \tilde{f}\left(\frac{n}{2^j}\right) e^{-2\pi i n k / 2^j}, \quad k = 0, ..., 2^j - 1. \quad (A.3)$$

Considering a 1-periodic function $\tilde{f}$, the coefficients of a DFT with 2^j entries are related to $\hat{\tilde{f}}(n)$ through the "aliasing relation"

$$\hat{\tilde{f}}_k = \sum_{z \in \mathbb{Z}} \hat{\tilde{f}}(k + 2^j z), \quad k = 0, ..., 2^j - 1. \qquad (A.4)$$

Finally, the transform

$$\tilde{f}^*(\omega) = \sum_{n \in \mathbb{Z}} f(n) e^{-2\pi i \omega n}, \quad \omega \in \mathbb{T}, \qquad (A.5)$$

is obtained from the sampled values of f. It fulfills

$$\tilde{f}^*(\omega) = \sum_{k \in \mathbb{Z}} \tilde{f}(\omega + k), \quad \omega \in \mathbb{T}, \qquad (A.6)$$

due to the Poisson summation formula. Equations (A.3)–(A.6) remain valid for $k \in \mathbb{Z}$, $\omega \in \mathbb{R}$, since $\hat{f}_k$ and $\hat{f}^*$ are periodic with period 2^j and 1, respectively.

ACKNOWLEDGMENT

REFERENCES

1. F. Arandiga and V. F. Candela, and R. Donat, *SIAM J. Sci. Comput.* **6,** 581 (1995).

2. E. Bacry, S. Mallat, and G. Papanicolaou, *Math. Mod. Num. Anal.* **26,** 793 (1992).

3. S. Bertoluzza and G. Naldi, *Comp. Appl. Math.* **13,** 13 (1994).

4. S. Bertoluzza and G. Naldi, preprint, Università di Pavia, 1994.

5. S. Bertoluzza and G. Naldi, *Appl. Comp. Harm. Anal.* **3,** 1 (1996).

6. G. Beylkin, R. Coifman, and V. Rokhlin, *Comm. Pure Appl. Math.* **44,** 141 (1991).

7. G. Beylkin, in *Progress in Wavelet Analysis and Applications, Proceedings of the International Conference Wavelets and Applications, Toulouse, 1992*, edited by Y. Meyer and S. Roques (Editions Frontiers, Gif-sur-Yvette, 1993), p. 259.

8. H. Bockhorn, J. Fröhlich, and K. Schneider. preprint, 1996.

9. R. Brand, W. Freeden, and J. Fröhlich, *Computing* **57,** 187 (1996).

10. J. D. Buckmaster and G. S. S Ludford, *Theory of Laminar Flames* (Cambridge Univer. Press, Cambridge, 1982).

11. W. Cai, and J. Wang, *SIAM J. Numer. Anal.* **33,** 937 (1996).

12. Ph. Charton and V. Perrier. *RAIRO Modél. Math. Anal. Numer.* **29,** 701 (1995).

13. C. K. Chui, *An Introduction to Wavelets* (Academic Press, Boston, 1992).

14. C. K. Chui and X. Shi, in *Mathematical Methods in Computer-Aided Geometric Design*, edited by T. Lyche and L. L. Schumaker, (Academic Press, San Diego, 1992), p. 111.

15. S. Dahlke and I. Weinreich, *Constr. Approx.* **9,** 237 (1993).

16. W. Dahmen and A. Kunoth. *Numer. Math.* **63,** 315 (1992).

17. I. Daubechies. *Ten Lectures on Wavelets* (SIAM, Philadelphia, 1992).

18. B. Denet and P. Haldenwang, *Combust. Sci. and Tech.* **86,** 199 (1992).

19. G. Deslauriers and S. Dubuc, *Constr. Approx.* **5,** 49 (1989).

20. D. L. Donoho, preprint, Stanford University, 1992.

21. B. Engquist, S. Osher, and S. Zhong, *SIAM J. Sci. Comput.* **15,** 755 (1994).

22. J. Fröhlich and K. Schneider, *Europ. J. Mech., B/Fluids* **13,** 439 (1994).

23. J. Fröhlich and K. Schneider, preprint, University Kaiserslautern, 1995; *Appl. Comp. Harm. Anal.,* to appear.

24. S. Gomes and C. Cuncha, preprint, Universidade de Campinas, Brazil, 1995.

25. A. Harten, *Comm. Pure Appl. Math.* **48,** 1305 (1995).

26. A. Harten, *SIAM J. Numer. Anal.* **33,** 1205 (1996).

27. S. Jaffard, *C.R. Acad. Sci. Paris I* **308,** 79 (1989).

28. S. Jaffard, *SIAM J. Numer. Anal.* **29,** 965 (1992).

29. B. Jawerth and W. Sweldens, *SIAM Rev.,* **36,** 377 (1994).

30. S. Lazaar, J. Liandrat and Ph. Tchamitchian, *C.R. Acad.Sci. Paris I* **319,** 1101 (1994).

31. P. G. Lemarié, *Rev. Math. Iberoamericana* **7,** 157 (1991).

32. P. G. Lemarié-Rieusset and G. Malgouyres. in *Wavelets and Applications,* edited by Y. Meyer (Masson, Paris, 1992).

33. J. Liandrat and Ph. Tchamitchian, Technical report, ICASE, 1990.

34. Y. Maday, V. Perrier, and J.Ch. Ravel, *C.R. Acad.Sci. Paris I* **312,** 405 (1991).

35. Y. Maday and J.Ch. Ravel, *C.R. Acad.Sci. Paris I* **315,** 85 (1992).

36. V. Maz'ya, in *The Mathematics of Finite Elements and Applications. Highlights 1993,* edited by J. R. Whiteman (Wiley, New York, 1994).

37. Y. Meyer, *Ondelettes et Opérateurs I/II* (Hermann, Paris, 1990).

38. V. Perrier and C. Basdevant, *Rech. Aérosp.* **3,** 53 (1989).

39. F. Plantevin, *Advances in Comp. Math.* **4,** 293 (1995).

40. P. Ponenti, Ph.D. thesis, University Aix-Marseille I, 1994.

41. Z. Qian and J. Weiss, *J. Comput. Phys.* **106,** 155 (1993).

42. P. Ronney, *Combust. Flame* **82,** 1 (1990).

43. I. J. Schoenberg, *J. Approx. Theory* **2,** 167 (1969).

44. G. I. Sivashinski, *Acta Astronaut.* **4,** 1177 (1977).

45. E. M. Stein and G. Weiss, *Fourier Analysis on Euclidian Spaces* (Princeton Univer. Press, Princeton, NJ, 1971).

46. W. Sweldens, preprint, IMI, Dept. of Math., Univ. of South Carolina, 1994.

47. W. Sweldens and R. Piessens, *SIAM J. Numer. Anal.* **31,** 1240 (1994).

48. Ph. Tchamitchian, *Rev. Mat. Iberoamericana* **3,** 163 (1987).

49. O. V. Vasilyev, S. Paolucci, and M. Sen, *J. Comput. Phys.* **120,** 33 (1995).

50. G. Walter, *IEEE Trans. Inform. Theory* **38,** 881 (1992).